7

The *in vacuum* diamond sensor

An *in vacuum* diamond sensor (DSv) was designed for beam core and beam halo measurement with large dynamic range. This DSv was characterized using the radioactive sources at CERN and tested using the electron beam at PHIL before the installation at ATF2. Further measurements were done at ATF2 to define the dynamic range and linearity response. In this chapter the we will describe the design of the DSv, the measurements we have done to characterize the DSv and discuss the different effects observed during the measurements.

7.1 Design of the *in vacuum* diamond sensor

For the measurements at ATF2, a large signal range from $10^2/mm^2$ for Compton and $10^4/mm^2$ for beam halo to $10^8/mm^2$ for beam core is required (see Table 7.1). As in first approximation the signal strength is proportional to the metallised surface of the electrode on the diamond, a geometry with four strips was adopted to help cover this large dynamic range (see Fig. 7.1). The two strips for beam halo scanning are on the two sides, with dimension 1.5 mm$\times$ 4 mm, and the other two in the center are for beam core scan, with dimension of 0.1 mm$\times$4 mm. Besides, one 0.5Ω resistor was added to one of the narrow strips (CH2) on sample No.1 to act as an current divider. On sample No.2 there is no 0.5Ω resistor. Sample No.1 was used for the tests at PHIL and sample No.2 was installed at ATF2 for the horizontal beam halo measurement.

Name	Total N	Max. N/mm^2	Charge signal/mm^2
Beam core	10^{10}	6.2× 10^8	1.7μC
Beam halo	10^7	2.2× 10^4	61.4pC
Compton	28340	5.2× 10^2	1.4pC

Table 7.1: Expected signal at DSv location at ATF2

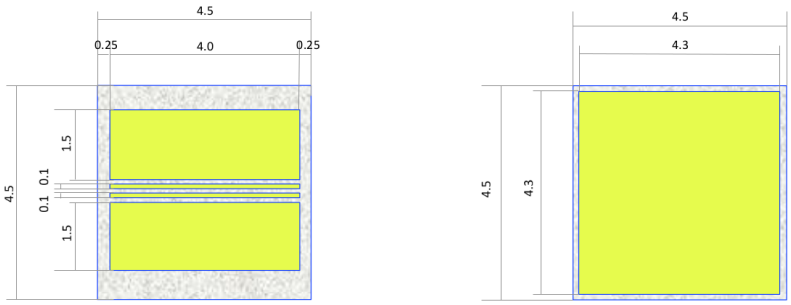

Figure 7.1: DSv with 4 strips:topside (left) and bottom side (right).

7.1.1 PCB and electrical circuit design

For the *in vacuum* application a ceramic PCB is used. The ceramic PCB uses silver-platinum conductor produced in thick-file technology. The PCB and the electrical circuit for the diamond detector is shown in Fig. 7.2, a low pass filter together with the charging capacitors are mounted on the backside of the ceramic PCB. The parameters of this circuit were set based on the following considerations:

- The cut-off frequency for high voltage power supply should be as low as possible to maintain the stability;
- The amount of charge stored on the capacitors should be large enough for measurements of large beam intensities, up to 1 μC on the narrow strips;
- The charging time constant should be small to enable separating successive bunches, the bunch repetition rate being 5 Hz at PHIL and 3 Hz at ATF2;

The simulated cut-off frequency for the present circuit is 8 Hz with 500 μC maximum stored charge at 500 V and the charging time constant is 44 ms.

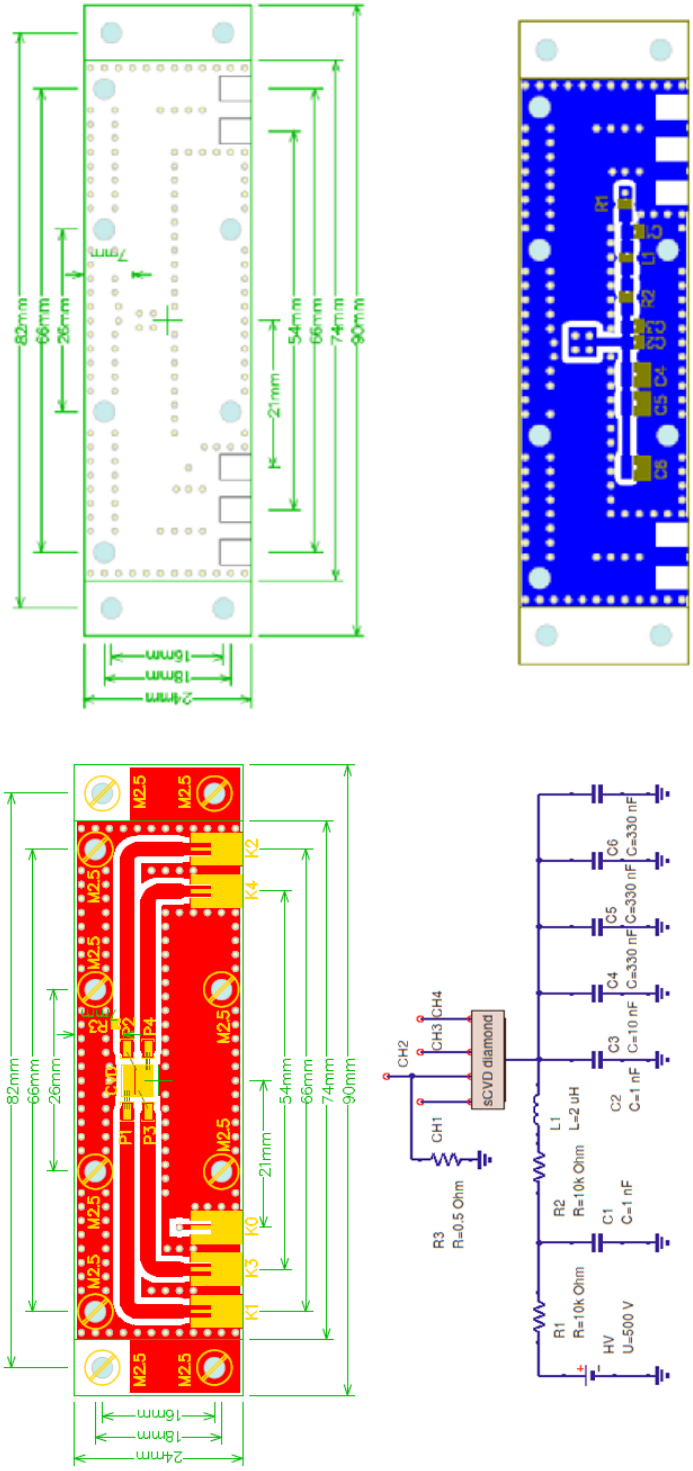

Figure 7.2: Layout of the PCB and electronic circuit for DS (sample No.1).

7.1.2 Mechanical design

The diamond sensor is designed to be installed in vacuum with a holder to scan the beam and beam halo. The mechanical design was done and fabricated at LAL as shown in Fig. 7.3. The whole setup is 744 mm long and it can be oriented either horizontally or vertically to scan in different axes. The vacuum chamber with an inner diameter of 72.1 mm is connected to the beam pipe, which has a diameter of 63 mm, installed after the BDUMP bending magnet at ATF2 via two DN63CF flanges. At ATF2 the DSv is inserted from the low energy (LE) side to the high energy (HE) side. This design is compatible for PHIL and ATF2. Therefore, it was installed and tested at PHIL before the implementation at ATF2.

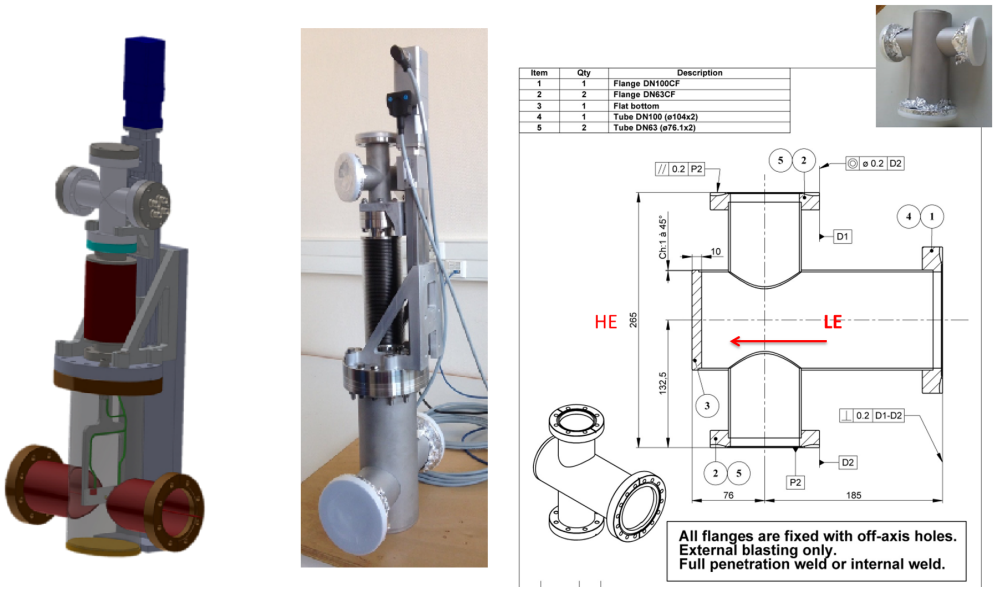

Figure 7.3: Left: Mechanical design; Middle: Fabricated mechanics; Right: Vacuum chamber layout.

7.2 Characterization of DSv

First tests of the DSv were done at CERN together with the CIVIDEC company in May 2014. The tests included the I-V curve measurements and the tests using radioactive sources. Then the DSv with the mechanics were installed at PHIL for the tests in vacuum using electron beams. In the tests, different strips are refereed to as different

channels. CH1 and CH4 represent the wide strips, CH2 and CH3 represent the narrow strips.

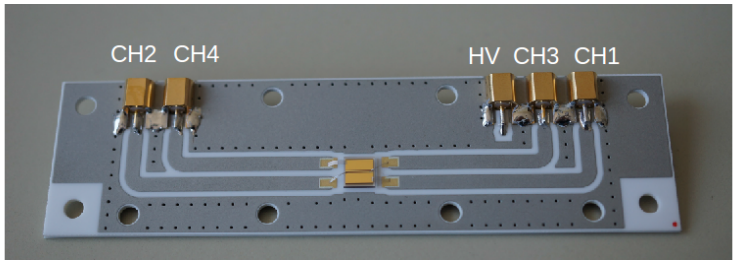

Figure 7.4: Photo of sample No.1 before adding 0.5Ω. CH1 and CH4 represent the wide strips, CH2 and CH3 represent the narrow strips.

7.2.1 I-V measurement

Prior to the I-V measurement, the dark current settling time is measured. Fig. 7.5 shows an example of the measured dark current setting process after applying 10 V and 50 V. It can be seen that, in this example, the dark current is setted after ∼5 s of waiting time for both cases. However, in our experiments the waiting time was set longer (⩾ 15 s) to ensure a stabilised dark current level.

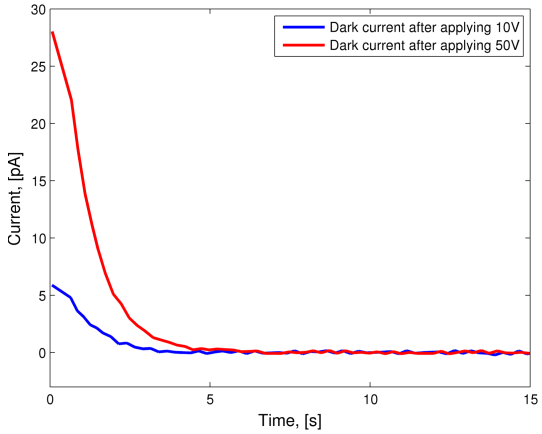

Figure 7.5: Settling of dark current after applying 10 V (blue) and 50 V (red) to CH1 of sample No.1.

For the measurement of sample No.1, we changed the bias voltage every 15 s with 50 V steps up to ±600 V. The current was recorded each 0.2 s, but only the data taken after the 15 s waiting time (∼20 points) were averaged to get the dark current

(see Fig. 7.6). However, for sample No.2, the dark current level was much higher than for sample No.1 and the settling time is also longer (>30 s) [1]. Therefore, we did the measurement by manually changing the bias voltage continuously [2].

Fig.7.6 shows the hysteresis loop of I-V dependence for CH1 of sample No.1 and CH4 of sample No.2. The measured dark current for CH1 of sample No.1 is below 0.6 pA. The other channels on sample No.1 had similar level of dark current. However, for sample No.2, the measured dark current level is ∼100 pA at +500 V and ∼60 pA at +400 V. This is 100 times higher than sample No.1, however, as long as the dark current is below nA level, it is acceptable, since the current generated by 1 MIP is ∼1 μA.

In principle the bias voltage applied to DSv can be raised to 1000 V, however, as the other components (resistors and capacitors) can only stand a bias voltage of 500 V, and as we have observed a sudden rise of dark current after applying more than 400 V for sample No.2, we defined the safe operation bias voltage range as $\pm 400V$.

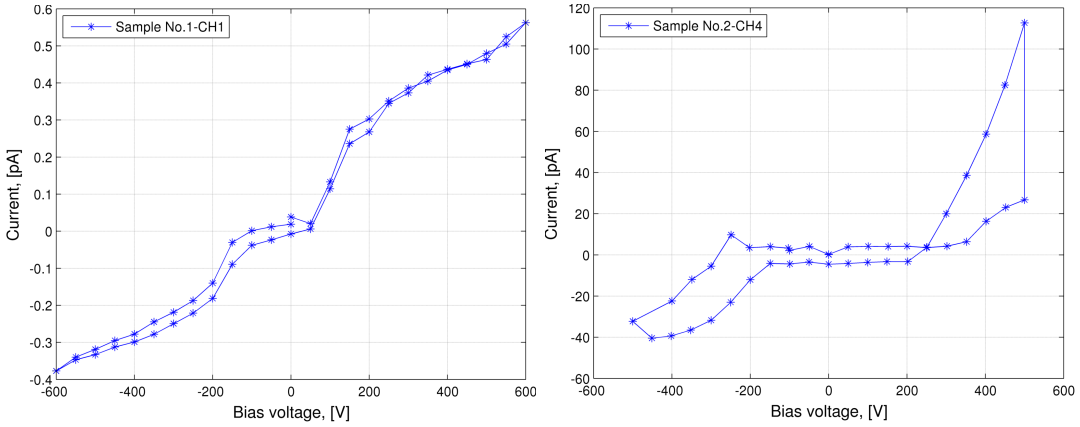

Figure 7.6: I-V measurement for CH1 of sample No.1 (left) and CH4 of sample No.2 (right).

7.2.2 Measurements using β source

Tests using β source were done for the two samples of DSv. Four 40 dB current amplifiers were used for the simultaneous signal readout of four channels.

[1] We assume this is due to the different level of impurity between the two samples, since the settling time and the dark current level are both related to the crystallographic defects inside the diamond bulk [115].

[2] The settling time is shorter by changing the bias voltage continuously than changing it by step.

The measurement set-up is similar to the one described in section 6.2.1. The β source was put on the top of each channels of DS. The signal was triggered on the tested channel and the signals from the other channels were displayed simultaneously. Fig. 7.7 and Fig 7.8 show the signal triggered on different channels for sample No.1 and sample No.2 separately.

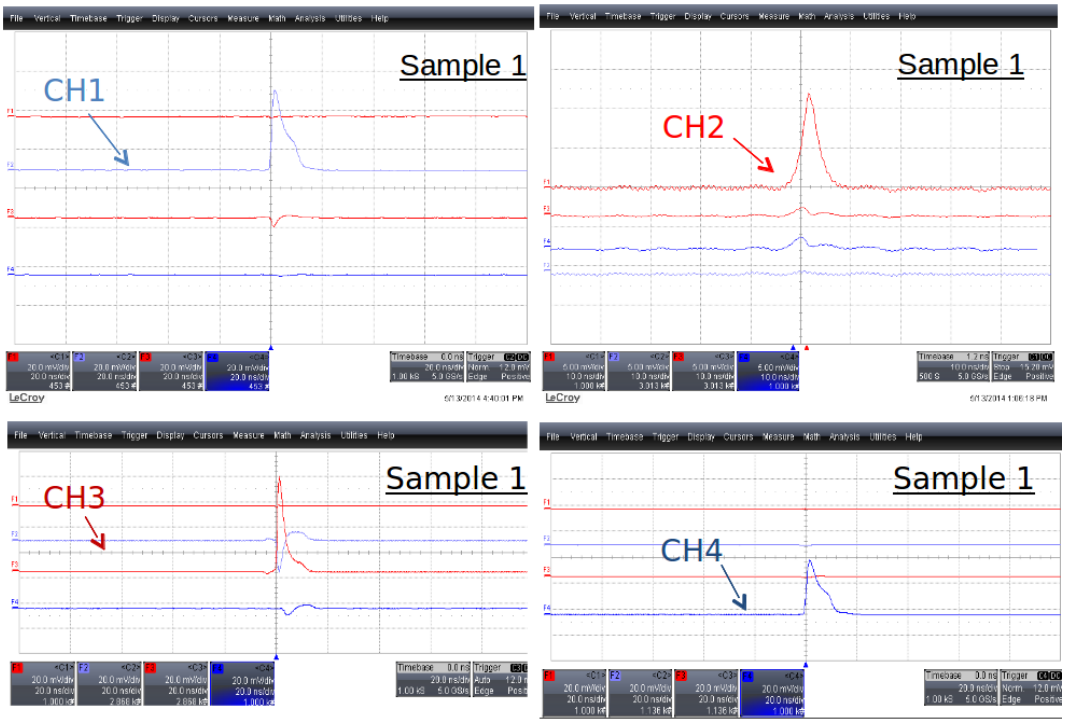

Figure 7.7: Tests of DSv sample No.1 using 90Sr source.

From these figures we can see that when the MIPs pass through one channel, small signal on the other channels can also be observed. The signals on the other channels are from the induced current due to capacitive coupling. This effect can be caused by the capacitance between the strips on the DS itself and by the capacitance between the signal readout lines on the PCB (see Fig. 7.4). Therefore, even though CH1 and CH3 is separated by CH2, as their readout lines are next to each other, CH3 has a stronger induced current than CH2 when the signal is triggered on CH1. The same effect can be seen when the signal is triggered on CH4 (see Fig. 7.8).

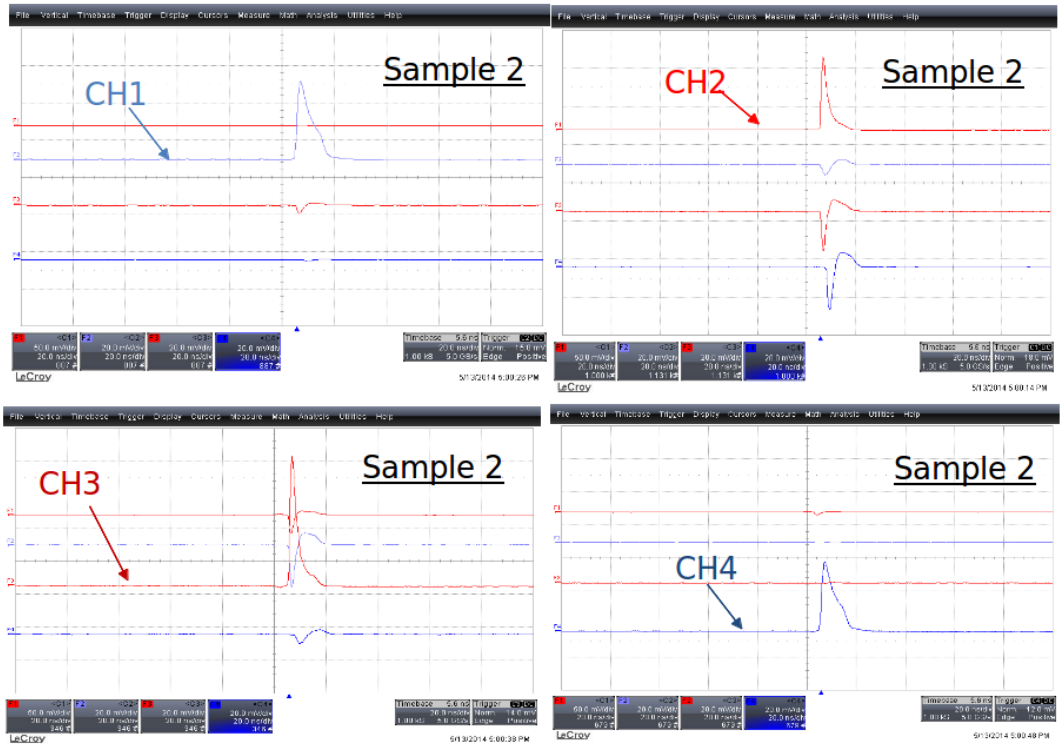

Figure 7.8: Tests of DSv sample No.2 using 90Sr source.

7.3 Tests of DSv at PHIL

The DSv was installed at PHIL in Sept.2014. It was installed horizontally in the end of beam line just before the exit window. The main purpose of the tests was to prepare our data acquisition system, test the motor system and verify the signal response on different channels of the DSv.

The experimental set-up is similar to the in air tests we have done at PHIL (see section 6.4.1). In order to test two channels at the same time in the control room, we added another cable line using 50 m 1/2 inch Heliax cable plus 50 m 1/4 inch Heliax cable. As we don't have additional Heliax cables, simultaneous tests for four channels were done by putting the Agilent scope inside the experiment hall and connecting to the DS using 2 m long RG58 coaxial cables.

In order to increase the maximum input signal voltage into the scope from 4 V to 40 V, four 50Ω terminators were added in parallel to the four channels on the scope. This enables the usage of 1MΩ input impedance on the scope with a maximum of 40

V input voltage.

7.3.1 Outgasing issues

After first installation we found an outgasing issue caused by the Allectra vacuum cables, which are used to transmit the signal from the PCB to the feedthrough (see Fig. 7.15). This issue prevented the vacuum to be pumped below 10^{-4} Pa. Since the main component of the gas was found out to be the water molecules, in order to mitigate the outgasing, the whole system was pre-baked before installation. This procedure allows to reach better than 5×10^{-6} Pa pressure as long as the time interval is not longer than four hours in air before installing and pumping again. This vacuum level is enough for the tests at PHIL with a Cu cathode, and also for the experiments at ATF2 in the Post-IP region, where the typical vacuum level is around 5×10^{-4} Pa. However for a permanent installation at PHIL, where other more sensitive photo-cathodes are used, vacuum level of about 10^{-7} Pa is required.

7.3.2 Signal pick-up and reflections

As the ceramic PCB, on which the DS is mounted, is not shielded, when the beam pass by/through the PCB, a bipolar current pulse is induced on the signal readout lines on the PCB. The signal given by the induced current is called pick-up signal.

Pick-up signal was observed during the tests using the DSv without applying a bias voltage. An example of pick-up signal waveforms is shown in Fig. 7.9. The integrated charge of pick-up signal is at the level of 1pC. This level of signal doesn't effect the beam core measurement with the signal level of 100 pC.

For the tests at PHIL, we applied -300 V bias voltage to the DS. Fig. 7.10 shows the waveforms obtained for the 4 channels when the beam is centered on CH1. An obvious periodical reflection with a delay of $\sim$30 ns can be seen on each channel. This reflection is due to the impedance mismatch of the 50 Ω terminators that we used to enable 1 MΩ input resistance in the scope. Tests of those 50 Ω terminators were done using the Time Domain Reflectometry (TDR) technique, which will be explained in Section 7.4.2.

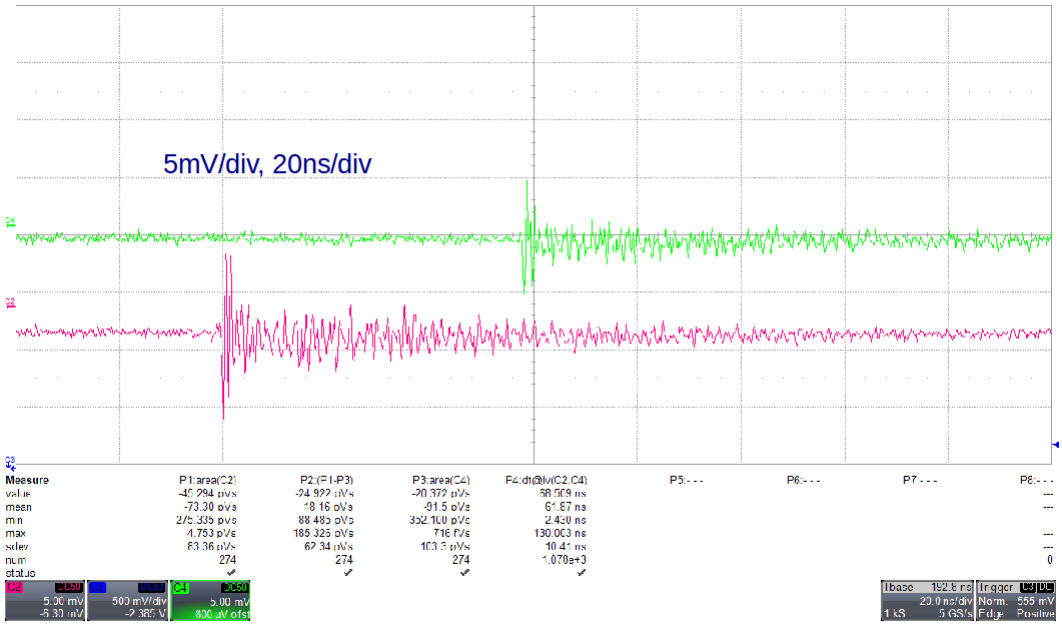

Figure 7.9: Pick-up signal from CH1 (red) and CH4 (green) at PHIL.

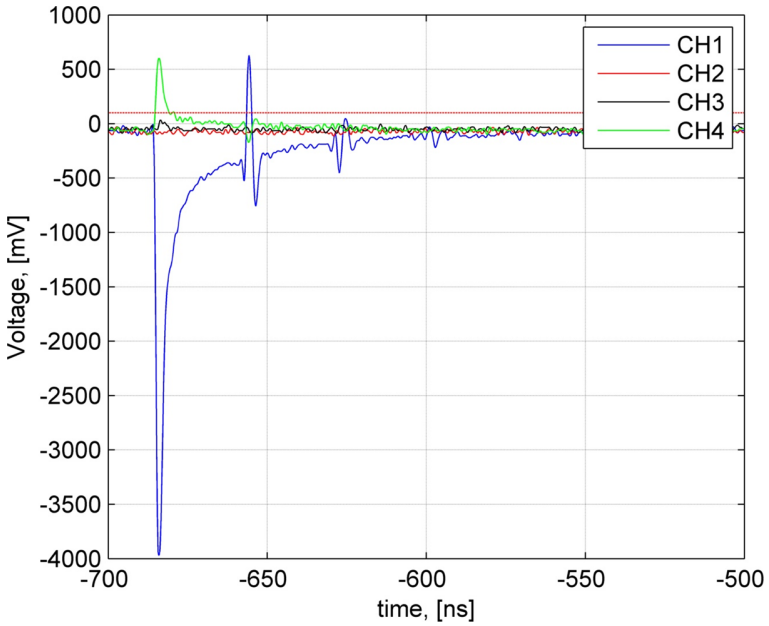

Figure 7.10: Signal waveforms on each channel with reflections.

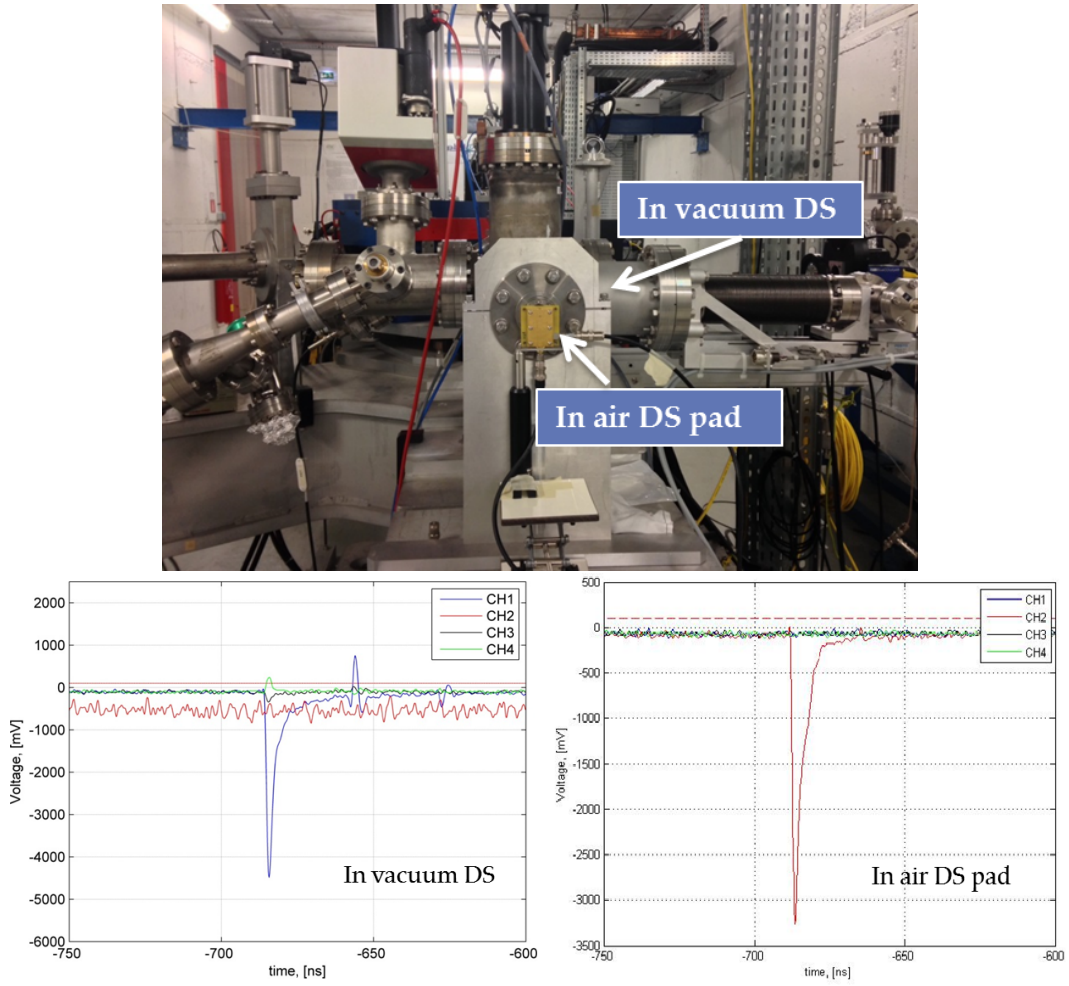

Figure 7.11: Tests at PHIL using two DS simultaneously: DSv and in air DS pad (data taken on 9th Oct.2014).

7.3.3 Beam core scan

After investigating the signal waveforms, it is important to verify the signal strength. As prior tests on DS pad (DS sample No.2) were done in air (see Section 6.3), and the signal was calibrated, it is worthy to compare the signal obtained from the DSv with that from the DS pad in air. Therefore, we installed the DS pad after the exit window as shown in Fig. 7.11. The distance between the DSv and the DS pad is around 133 mm. Both the DSv and the DS pad were connected to a 12 dB attenuator. The beam is aligned vertically using the steerer upstream. The input beam intensity is 62 pC and the beam size measured at the YAG3 screen, which is 22 cm upstream of DS, is

σ_x=1.57±0.08 mm and σ_y=1.92±0.06 mm. The bias voltage applied on the DSv and DS pad is -300 V.

In Fig. 7.11 lower left plot shows the signal on each channel when the beam is centred on CH1, and the lower right plot shows the signal on the in air DS pad. It can be seen that the signal amplitude in the same order (-4.5 V for CH1 and -3.25 V for the DS pad). Although the DS pad has a larger surface than CH1, as the beam is diverging both in X and in Y, the signal level on the DS pad in air can be smaller than CH1.

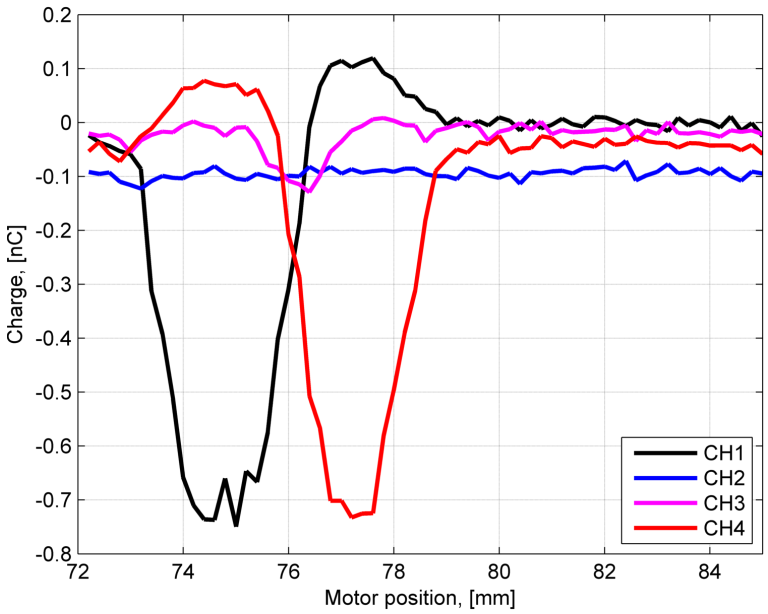

Figure 7.12: Beam core scan using 4 channels of DSv at PHIL(data taken on 9th Oct.2014)

Beam core scan using the DSv were done by applying -300 V of bias voltage. The integrated charge of the waveforms is plotted during the scan. The distribution of the integrated charge is shown in Fig. 7.12. As CH2 is connected to a 0.5 Ω, and the scope resolution is not optimised for this channel, the distribution on CH2 is almost flat. However, for the other channels we can clearly see the negative peaks which indicate the signal level when the beam passes through the center of each channel. The distance between these peaks corresponds well to the distance between the centers of different channels.

Beside, positive peaks can also be seen from the distribution. The origin of which is under investigation.

7.4 Experimental set-up at ATF2

The first set of DSv was installed at ATF2 in Nov.2014. It was installed horizontally for the purpose of measuring the horizontal beam halo distribution and investigating the possibility of measuring the Compton recoil electrons, which are distributed on the low energy side after the BDUMP bending magnet.

7.4.1 Data acquisition system

For the reason of radiation safety, the oscilloscope and other readout electronics were located in the IP laser room outside the tunnel. Therefore, in order to collect the signal from the DSv at Post-IP region, we used LDF1-50 1/4 inch thick Heliax coaxial cables (more than 20 m).

Fig 7.13 shows the experimental set-up for data taking which includes the power supply, motor control and oscilloscope. For the bias voltage supply we used the Keithley 2410 sourcemeter, which can supply a bias voltage of $\pm$1000 V. The whole data acquisition system is connected via Ethernet cables to the PC located in the control room. On the PC, a Matlab program is installed and used for the data taking. The oscilloscope we used is an Agilent oscilloscope with a sampling rate of 4 GS/s and an analogue bandwidth of 1 GHz. The motor we used for DSv scanning is a stepper motor EMMS-ST-42-S-SEB-G2 fabricated by the Festo company. This stage is driven by a ball bearing spindle of 2 mm pitch for one revolution. The stepping motor performs one rotation by 200 steps (stepper angle 1.8$\pm$5%). Combining the ball bearing spindle and the precise stepping motor, the resolution of the steps is 10 μm and the repetition accuracy is up to 3μm. The precision we set in the Matlab program is 50 μm.The maximum scan distance is 110 mm. The moving speed and acceleration can be adjusted. This motor can be controlled via a commercially developed software called "Festo". Also one can check the status of the motor via the web interface. However for the integration into the control system, we used the Matlab program to connect to the motor and use web commands to control the motor. In our program we used two moving speed, one with 1 mm/s for fast moving before reaching the destination

with a resolution of 100 μm, and once this resolution is reached, we use a slower speed (crawling velocity) of 0.25 mm/s to adjust the position up to 50μm of resolution. The acceleration was set to 0.2 m/s^2.

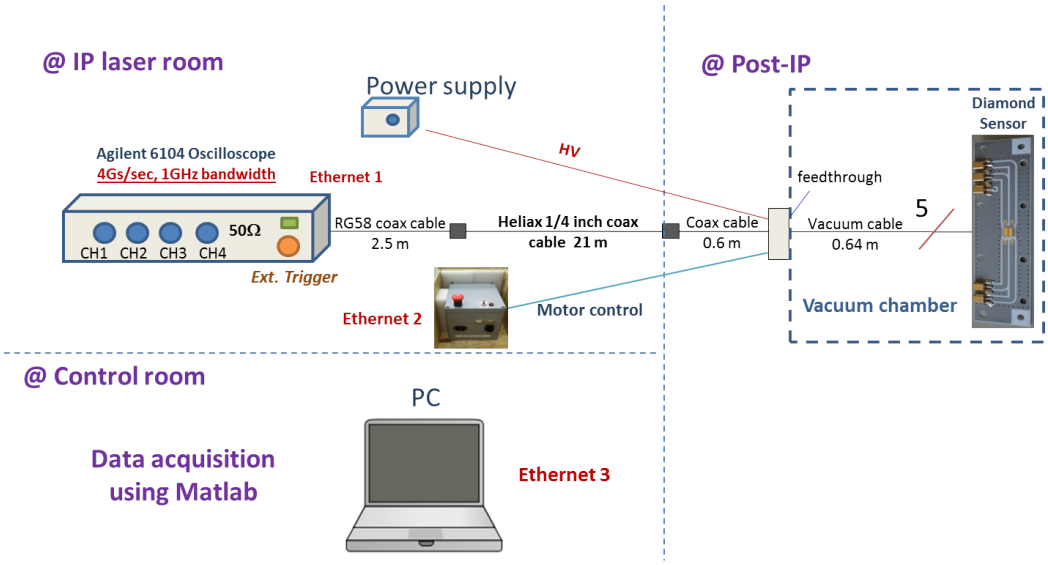

Figure 7.13: Layout of data acquisition system

In order to calibrate our DSv signal using the ICT measured charge and also verify the beam jitter level at the DSv location, we connected to the EPICS [124] system via SSH on Matlab and read data simultaneously from the ICT located after the BDUMP bending magnet and from the C-band BPM "MPIP" located after the IP. Fig. 7.14 shows the data taken via the EPICS system during the DSv scan. The data is synchronised to the DSv data pulse to pulse.

7.4.2 TDR measurements and impedance matching

In order to define the length of the cables and the impedance matching level of the whole system, Time Domain Reflectometry (TDR) measurements were performed using the Tektronix 80E04 TDR module. Time Domain Reflectometry (TDR) measures the reflections that result from a signal travelling through a transmission environment (e.g. a circuit board trace, a cable, a connector and so on) [125]. TDR measurements are described in terms of a Reflection Coefficient, ρ. The coefficient ρ is the ratio of the reflected pulse amplitude to the incident pulse amplitude:

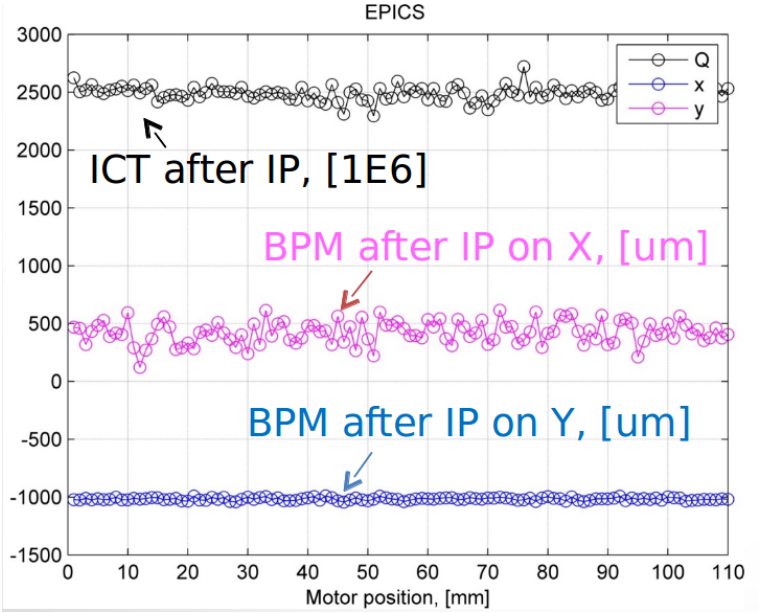

Figure 7.14: ICT and BPM data reading from EPICS system during the scan

$$\rho = \frac{V_{reflected}}{V_{incident}} \tag{7.1}$$

For a fixed termination Z_L,ρ can also be expressed in terms of the transmission line characteristic impedance, Z_0 and the load impedance Z_L.

$$\rho = \frac{V_{reflected}}{V_{incident}} = \frac{(Z_L - Z_0)}{(Z_L + Z_0)} \quad with \quad Z_L = Z_0 \frac{1+\rho}{1-\rho} \tag{7.2}$$

where $Z_0 = 50\Omega$ in our case. If there is no reflection, then ρ=0 and $Z_L = Z_0$. When there is a short circuit, then ρ=-1 and Z_L=0. When there is an open circuit, then ρ=1 and $Z_L = \infty$.

Figure 7.15 shows the TDR measurement for the DSv No.1 by connecting each channel to the TDR module using the 64 cm long Allectra vacuum cable, which is used to transmit the signal from the PCB to the feedthrough. The measurement result is shown in Figure 7.15 bottom. As CH2 is connected to a 0.5 Ω the response is close to a short circuit. The valley in the plot shows the impedance mismatch of the PCB. The difference of the valley width between CH1 and CH4 indicates the different length of path on the PCB.

The mismatch of impedance will cause the reflection of signals along the transmission line. This effect can be observed in the signal waveforms in Fig. 7.10 and Fig. 7.17.

The measurement for the experimental set-up with all the cables is shown in Figure 7.16.In our experiment, we have used the 1/4 inch LDF1-50 Heliax cable (with foam polyethylene dielectric), RG58 coax cables (with solid polyethylene dielectric) and vacuum cable (with kapton dielectric).

The velocity of signal propagation in the coaxial cable depends on the material of the insulator surrounding the inner conductor. The ratio between the transmission velocity in the cable and the speed of light is called the velocity factor (VF), which can be calculated as:

$$\mathrm{VF} = \frac{1}{\sqrt{\kappa}} \tag{7.3}$$

where κ is the dielectric constant (relative permittivity).

For the foam polyethylene dielectric, the VF is 82% and for the solid polyethylene dielectric and kapton dielectric it is 66% and 58.7%(?) respectively. Knowing the signal propagation speed and signal reflection time measured by TDR, we can calculate the length of the cable.The measured lengths of the cables are indicated in the figures (see 7.16).

TDR measurements were also done for the 50 Ω terminators that were connected to the scope to enable the usage of 1 MΩ input impedance on the scope, which increases the maximum input signal voltage from 4V to 40V. The tests result shows that the 50 Ω terminators that the impedance mismatch caused by the 50 Ω terminators is much higher than the mismatch of cables and PCB. Besides, as the 50Ωs terminators are connected to the end of the signal transmission line, the reflected signal has a delay of Δt=2*L_t/(C*VF), where L_t is the total cable length and C is the speed of light.

The estimated delay for the system is around 200ns for the setup at ATF2 and this reflection can easily be seen on the signal waveforms as shown in Fig. 7.17.

7.4.3 Scope vertical range setting

The scope resolution depends on the vertical range (VR) applied on the scope setting. The Agilent scope we used has a vertical resolution of 8 bits and a vertical sensitivity

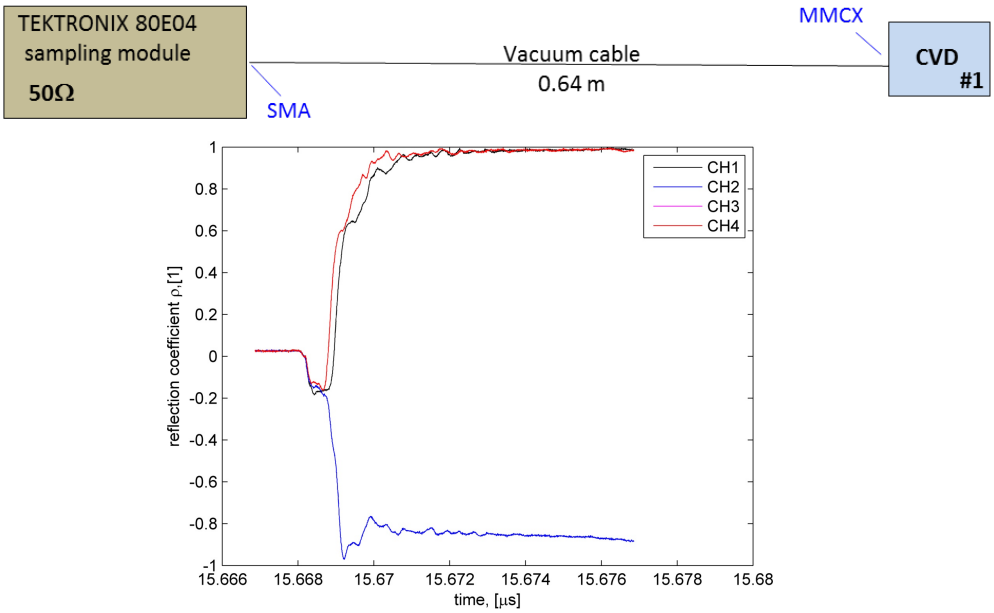

Figure 7.15: Top: Layout of TDR measurement for DSv No.1;Bottom : TDR measurement result for DSv No.1.

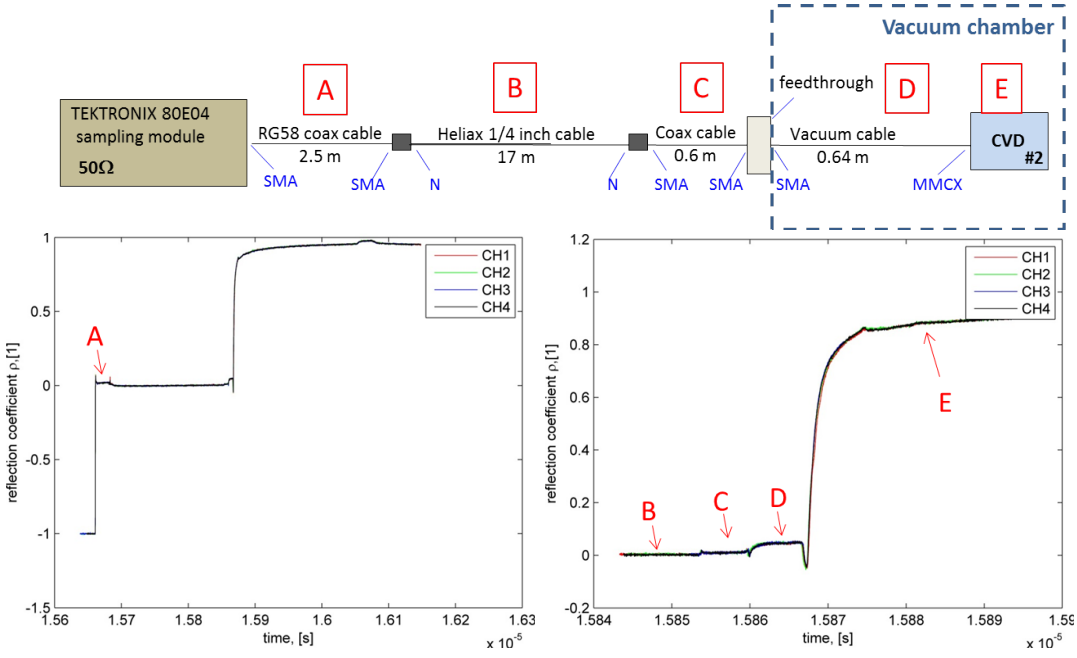

Figure 7.16: Top: Layout of TDR measurement for DSv Sample No.2; Bottom: TDR measurement result for DSv Sample No.2.

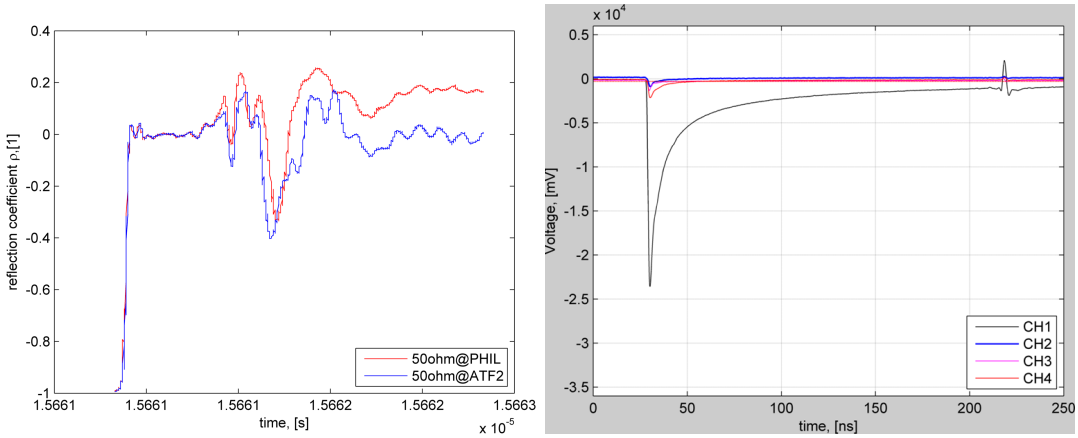

Figure 7.17: TDR test result of 50Ωs terminators (left) and signal reflection observed on the signal waveforms (right).

from 2 mV/div to 5 V/div. The measurement resolution of the scope can be calculated as:

$$Resolution = \frac{VR}{2^8} \tag{7.4}$$

Therefore for the minimum scope range 2mV/div, we have the maximum measurement resolution of 62.5 μV.

For the measurements of beam halo, as a large dynamic range is required, the scope VR should be adjusted for different measurement range. To achieve this, one can either set the VR manually for a certain range of scan and change it for another range or change the VR at each position automatically as will be explained in the next paragraph. Fig. 7.18 shows the difference of these two VR setting methods. By changing the VR manually at each range, we observe a distribution with several steps, and normalization between the steps will be needed as done for the measurements using wire scanners (for the data taken at different bias voltage). However, by changing the VR automatically at each position, a continuous beam halo distribution can be obtained.

Fig. 7.19 shows the distribution of VR set for the scope during the beam halo scan. In the program, at each point we set three VRs: 50 mV, 500 mV and 5 V to test which VR gives the best signal to noise ratio (SNR) without going into saturation, then we take the amplitude measured at this VR and multiply it by factor 4. In this way, the

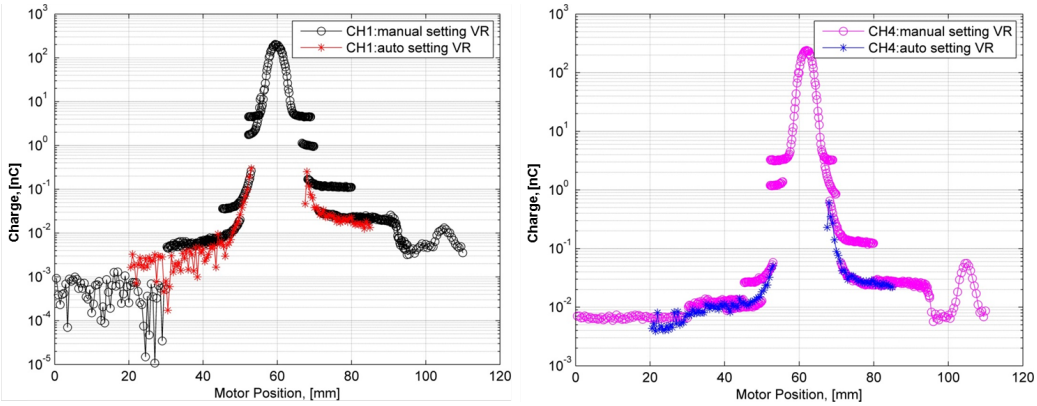

Figure 7.18: Comparison of beam halo scan between manual and auto setting scope VR for CH1 and CH4.

signal fills 1/4 of the full screen with certain offset. However, from Fig. 7.19 we can see that:

1) On the two edges of the beam halo, as the signal amplitude is given by the pick-up signal, the setted VR is relatively large. At 0 mm position, when the DS is completely out from the beam, the VR is $\sim$ 0.2 V. According to Equation 7.4 the measurement resolution is then 0.78 mV, which corresponds to a noise level of $\sim$100 electrons supposing a signal FWHM of 10 ns. Therefore, without signal pick-up, we would expect the noise level to be much lower.

2) Near the beam core, when the signal reaches the limit of the screen (20 V w/o offset) during the test, the output VR will be 80 V which is more than the limit of the VR (40 V), then the VR is set to 40 V by default. This explains the saturation level of 40 V as shown in Fig. 7.19. To avoid the saturation of VR, the scan range should be set with care (normally $> 3\sigma$ or $< -3\sigma$). In the data analysis, data taken with a saturated VR (if exist) are excluded from the distribution.

7.5 Characterisations of DSv at ATF2

Characterisation of DSv was done at ATF2 to define the dynamic range of the DSv. The lower limit of the dynamic range is defined by the noise level given by the pick-up signal and the higher limit will be impacted by the linearity of DSv response.

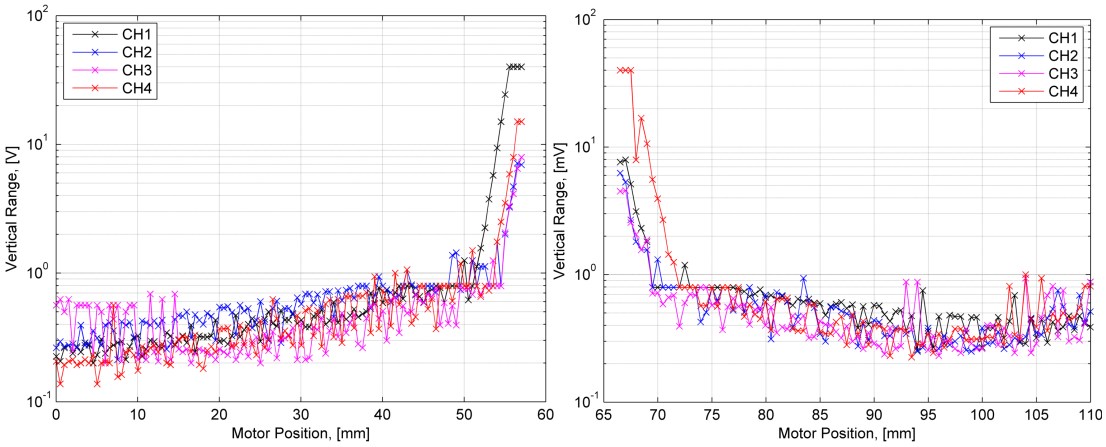

(a) **(b)**

Figure 7.19: VR distribution during the scan of beam halo on the left (a) and right (b) side.

7.5.1 Signal pick-up study

In Fig. 7.20 the pick-up signal on each channels is shown. The integrated charge of the pick-up signal during the scan is also shown. This scan was done without applying bias voltage to the DSv (by turning off the power supply). However, as the measurement was done after beam halo measurements with 400 V, and the bias voltage was ramped down from 400 V to 0 V in a relatively short time($\sim$ 30 s), the charging capacitors may not have totally discharged. Therefore, when the beam went through the DSv small amount of charge ($\sim$ 10 nC) was still collected as shown in the distribution.

Meanwhile, the integrated charge from pick-up signal is below 3×10^{-3}nC which correspond to 10^3 electrons. This defines the lower limit (noise level) of beam halo measurement for our present set-up. This level of noise affects our measurements in the following two aspects:

1) Covers the signal from Compton recoil electrons that we want to measure in the future.

2) Prevent us from seeing the tail of the waveform shape, where a small signal from backscattered particles from the DUMP is expected.

For the first effect, we need to avoid the pick-up signal in the measurements, therefore shielding of the PCB will be required. The shielding procedures are under discussion together with the CIVIDEC company.

For the second effect, as the pick-up signal has a much higher frequency than our signal, we can add a low pass filter (LPF) in data analysis to recover the signal waveforms.

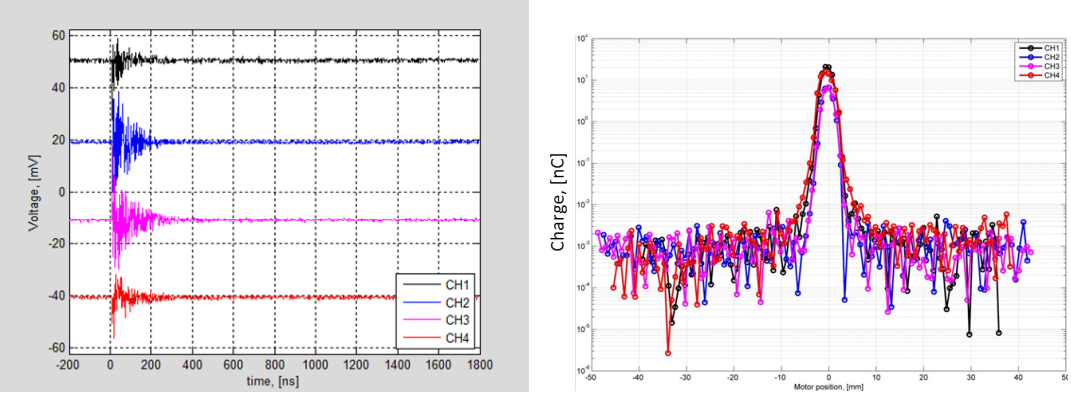

Figure 7.20: Pick-up signal on each channels (left) and integrated charge during the pick-up scan (right) taken on 8th Dec. 2014.

7.5.2 Fast Fourier Transform and Low Pass Filter

Fast Fourier Transform (FFT) is an algorithm for transforming data from the time domain to the frequency domain. In frequency domain, we can see clearly the frequencies of different components of the signal that we have measured. In Fig. 7.21 the FFT of signal waveforms from CH1 is shown for different range of motor positions during the pick-up scan as shown in Fig. 7.20. Except for the waveforms near the beam core region (50-70 mm) where the distribution is dominated by the lower frequency signal [1], we can find a common peak at around 0.3 GHz position in the other positions, we suppose that this frequency correspond to the pick-up signal frequency.

With a Low Pass Filter (LPF), the signals with frequency higher than the defined cutoff frequency (known as stopband) are attenuated, and only the signals below the cutoff frequency can pass through without attenuation. By removing some frequencies, the filter creates a smoothing effect. That is, the filter produces slow changes in output values to make it easier to see trends and boost the overall signal-to-noise ratio with minimal signal degradation [126]. Fig. 7.22 shows an example of the signal before and

[1] In the beam core region, the waveform is similar to the signal waveform, rather than the pick-up signal, since small amount of charge is collected as shown in Fig.7.20 (right).

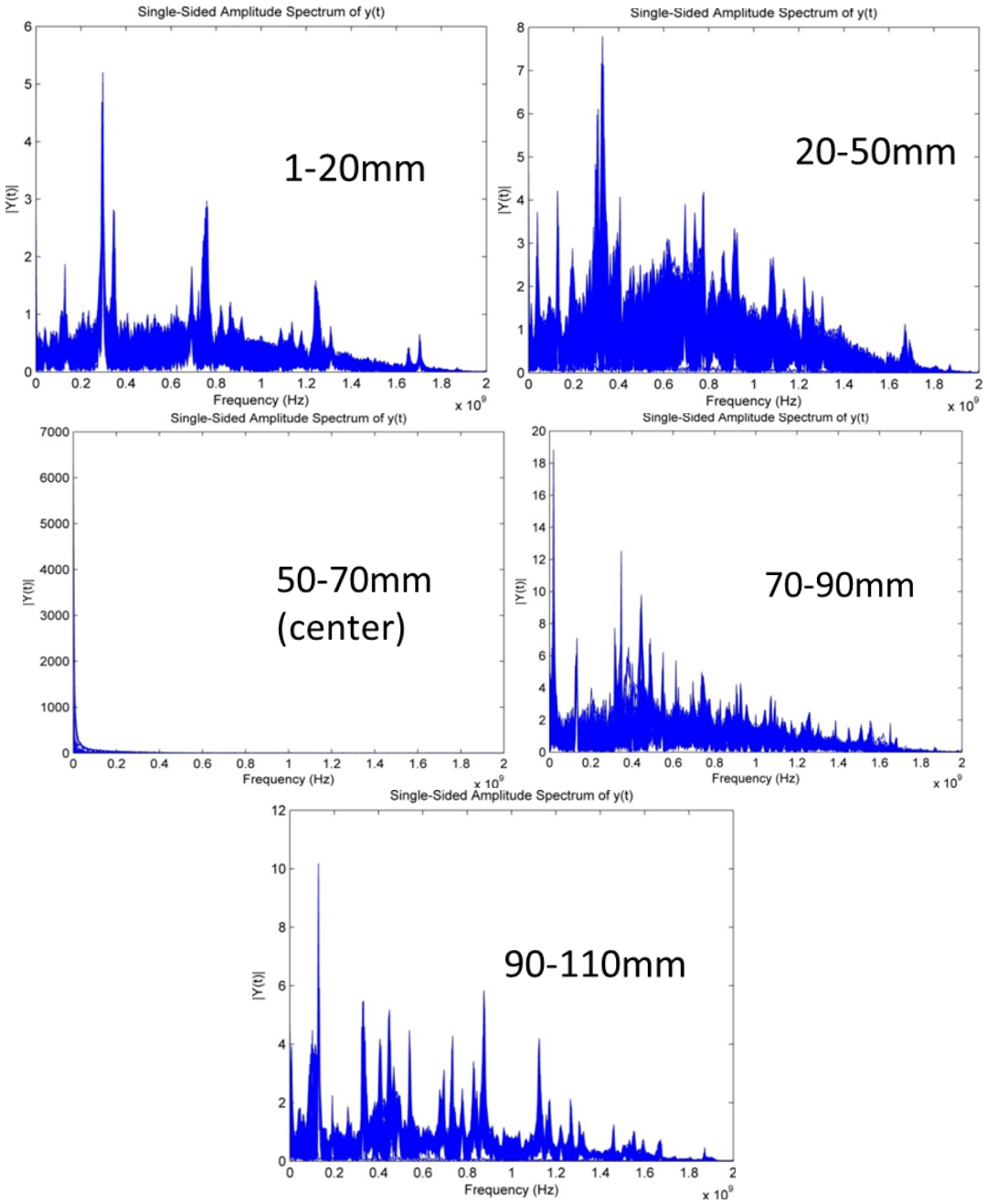

Figure 7.21: FFT of signal waveforms at different range of motor positions during the pick-up scan.

after applying LPF. The LPF applied is a 1-D digital filter with a cutoff frequency of 0.2GHz.

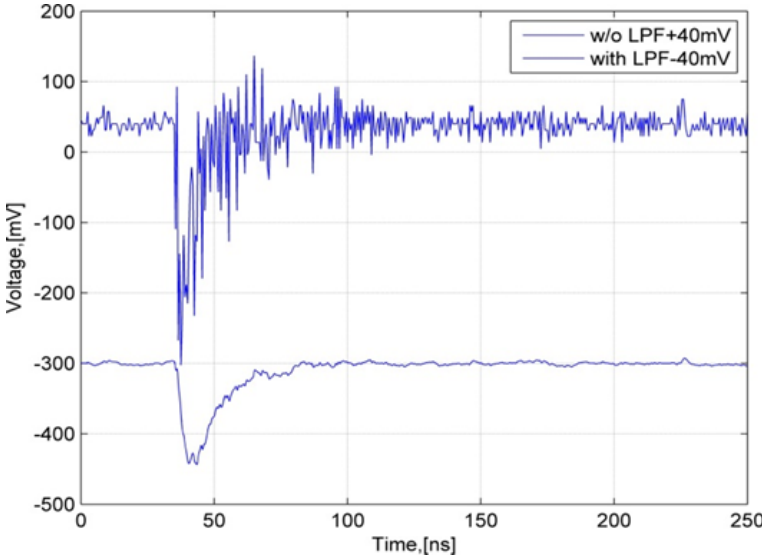

Figure 7.22: Signal waveform before and after applying LPF.

7.5.3 Signal Convolution

In Section 3.3.3 we have mentioned that the wire scanner measured distribution can be considered as a convolution of a cylindrical distribution and a Gaussian distribution. For the measurements using DSv strips, we can similarly consider the measured distribution ($S(\xi)$) as the convolution of a uniform distribution ($L(x)$) and a Gaussian distribution ($I(x)$).

The uniform distribution can be expressed as:

$$L(x) = \begin{cases} 1 & |x| \leq \frac{l}{2} \\ 0 & |x| > \frac{l}{2} \end{cases} \quad (7.5)$$

where ℓ is the width of the DSv strips.

The Gaussian distribution with maximum intensity of I_0, beam size of σ and mean value of μ can be expressed as:

$$I(x) = I_0 e^{-\frac{(x-\mu)^2}{2\sigma^2}} \quad (7.6)$$

Therefore, we can get the convoluted signal at position $x = \xi$, which can be expressed as:

$$S(\xi) = K(L * I)(\xi) = \int_{-\infty}^{\infty} KL(x-\xi)I(x)\,\mathrm{d}x \quad (7.7)$$

where K is a constant.

The convolution of the uniform and the Gaussian distribution ($S(\xi)$) can also be expressed using the error functions [1] as shown in Equation7.8. This equation is used for the beam core fit in the Matlab program to get the beam size σ after the beam core scan.

$$S(\xi) = KI_0 \int_{-\xi-\frac{l}{2}}^{\xi+\frac{l}{2}} e^{-\frac{(x-\mu)^2}{2\sigma^2}} \,\mathrm{d}x = KI_0(erf(\frac{\xi+\frac{l}{2}-\mu}{\sqrt{2}\sigma}) - erf(\frac{\xi-\frac{l}{2}-\mu}{\sqrt{2}\sigma})) \tag{7.8}$$

7.5.4 Linearity of DSv response

The linearity of DSv response is consider as one of the most important characterization aspects as it defines the linear region of operation and provides corresponding normalization factor for the calibration in the non-linear region.

In order to check the linearity, the beam intensity should be changed. This can be done in two ways: 1) change the input laser intensity for the photo-cathode; 2) change the DSv position in the beam core.

As the ICT sensitivity is above 10^9 electrons, the beam intensity below 10^9 can not be measured correctly. Thus in order to get to the lower beam intensity we have to change the DSv position in the beam core. At each position we changed the beam intensity from 10^9 to 7×10^9 electrons and took 100 waveforms for each beam intensity. Two campaigns of measurements were done in Dec.2014. Before the measurement, the beam was aligned vertically as described later in chapter 8.2.1, and then beam core was scanned horizontally and fitted according to Eq. 7.8 to get the horizontal beam size (see Fig. 7.23 (a)).

For the number of incident electrons calculation, similar to the measurements done at PHIL, as the beam core follows Gaussian distribution, the number of electrons intercepted on each channel N_{CH} at different positions can be calculated by adding a horizontal offset (d_x) to formula 6.19 as shown below:

$$N_{CH} = \frac{N_t}{2 * \pi * \sigma_x * \sigma_y} \int_{-\frac{1}{2}l_x+d_x}^{\frac{1}{2}l_x+d_x} e^{-\frac{x^2}{2\sigma_x^2}} \,\mathrm{d}x \int_{-\frac{1}{2}l_y}^{\frac{1}{2}l_y} e^{-\frac{y^2}{2\sigma_y^2}} \,\mathrm{d}y \tag{7.9}$$

The horizontal beam size in the formula is the measured beam size by DSv, which can be obtained from the fit of the beam core. However, as the vertical beam size

[1] Error function is defined as: $erf(x) = \frac{x}{\sqrt{\pi}} \int_0^x e^{-t^2} \,\mathrm{d}t$.

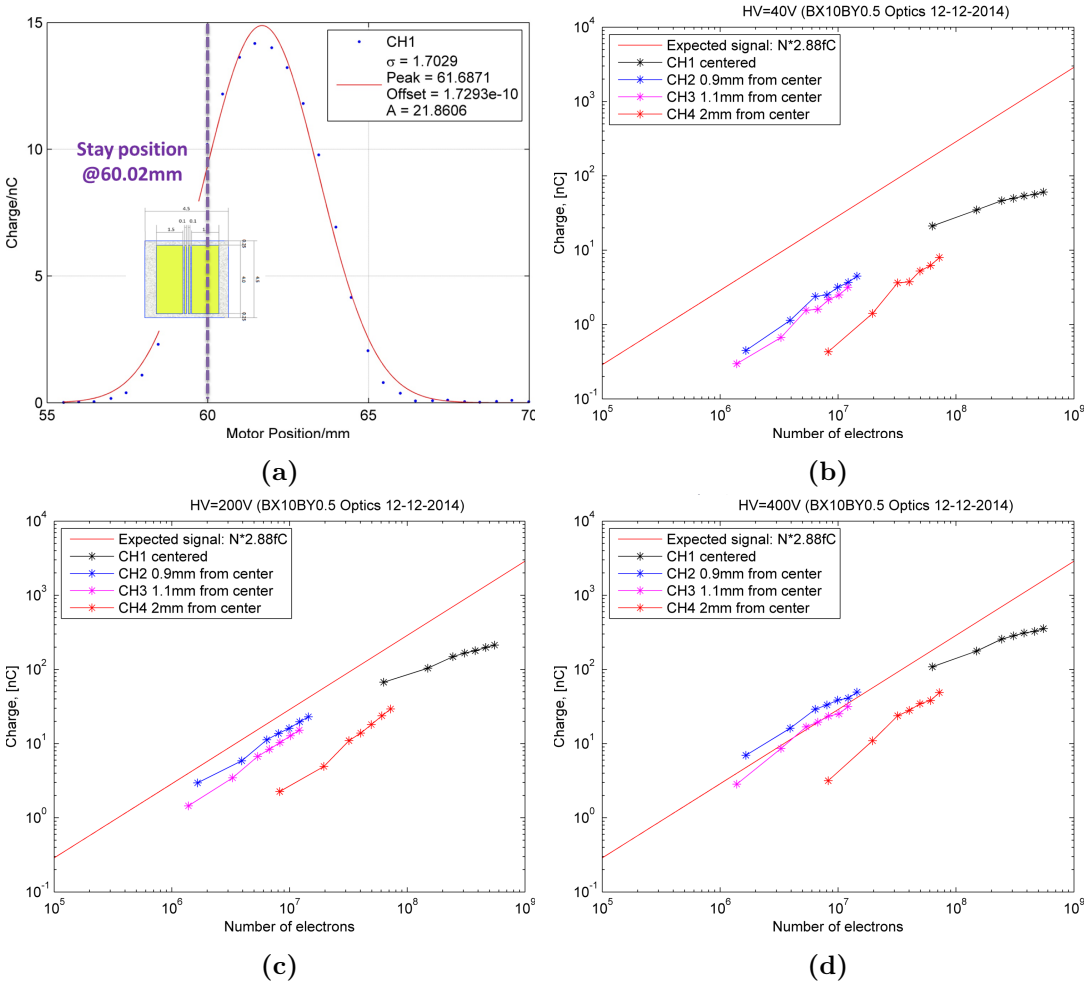

Figure 7.23: The position chosen for the linearity measurements (a) and the measurement results for the bias voltages of 40 V (b), 200 V (c) and 400 V (d) (data taken on 12-12-2014 with BX10BY0.5 Optics).

can not be measured at the DSv location, it can be obtained either by simulation using Madx or by extrapolating from the Post-IP measured beam size. The difference between the two methods are compared in section8.4.4.

For the first measurements the DSv was put at 1σ away from the beam core as shown in Fig. 7.23 (a). The bias voltage was changed from 40 V to 200 V and 400 V to investigate the change of Charge Collection Efficiency (CCE) as a function of bias voltage. From Fig. 7.23 it can be seen that by increasing the bias voltage, the collected charge is increased which indicates an increasing CCE.

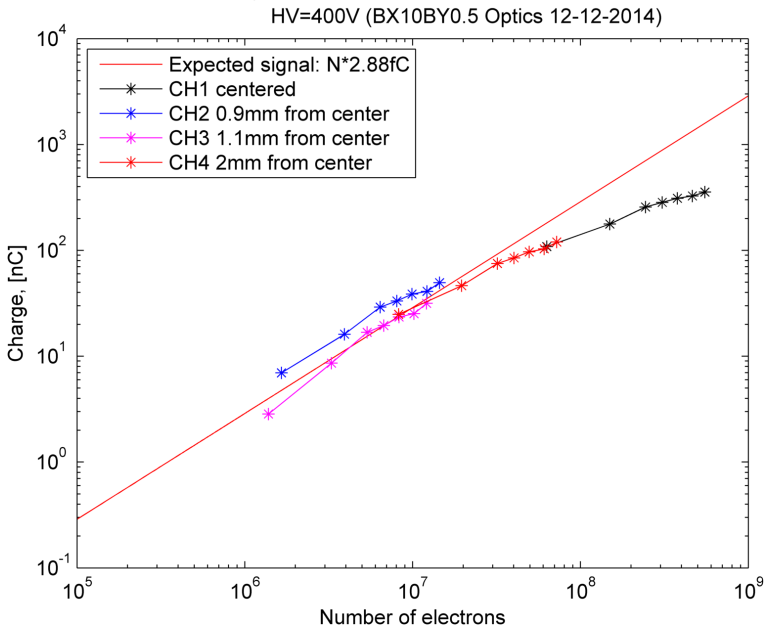

Figure 7.24: Correction for charge collected on CH4 for 400V of bias voltage.

The charge collected by CH2 and CH3 seems quite consistent with CH1, on which the slope start to deviate from the expected value. However, signal on CH4 seems much less than what we expected. This might be the caused by the same effect as what we have observed at PHIL. When high intensity beam go through one channel, there is an inverted signal on the other channels, then the measured signal on the other channels is the combination of the inverted signal and the beam generated signal. From Fig. 7.12 we can see that the inverted signal level is about 20% of the measured signal on the channel which is centered. After adding the 20% of signal to CH4 in Fig. 7.23, the signal on CH4 then becomes much more consistent with signal on other channels as shown in Fig. 7.24.

From Fig. 7.24 we can see that the deviation of signal from expected value starts at the beam intensity of 10^7. This can be explained by the voltage drop on the 50 Ω resistor on the scope. This voltage drop (V_{drop}) is proportional to the number of input electrons and it will reduce the effective bias voltage on the DSv (V_{eff}), which can be defined as:

$$V_{eff} = V_{bias} - V_{drop} \tag{7.10}$$

V_{drop} can be read out directly from the waveforms on the scope and it changes together with the current. Fig. 7.25 shows the signal waveforms of CH2 and CH4 in the beam center. The calculated number of input electrons (N_{CH}) using Eq. 7.9 is $\sim 10^7$ and $\sim 10^8$ for CH2 and CH4, respectively. From the waveforms it can be seen that, immediately after the passage of high intensity beam, a sudden rise of current is induced due to the fast movement of electrons and holes in the externally applied electric field (reaching rapidly their saturation velocities (v_{sat})). The instantaneous current generated by the N_{CH} input electrons can be calculated using the Shockley-Ramo formula (see Eq. 7.11) as:

$$I = E_v q v_{sat} \quad with \quad q = N_{CH} \times 2.88\ fC \tag{7.11}$$

where E_v is the normalized electric field. Assuming an averaged saturation velocity of $v_{sat} \approx 100 \mu m/ns$ according to our measurements results for the in air DS (see Table **??**), an instantaneous current of $I \approx 5.76A$ can be obtained for $N_{CH} = 10^7$, which corresponds to ∼288 V of output voltage. This calculated output voltage is quite consistent with the signal amplitude for CH2 as shown in Fig. 7.25 (a).

However, immediately after the arrival of this instantaneous current at the 50Ω resistor, a large voltage drop (∼288 V) is created, result in an effective bias voltage of $V_{eff} \approx 112V$. Since the CCE depends on the V_{eff} (see Fig. 6.15 (b)), when large voltage drop happens the drift velocity of electrons and holes are decreased, the charge collection time is extended, which increase the recombination probability and consequently less charge is collected. This increase of charge collection time can be observed from the long tail in the waveforms in Fig. 7.25.

Except for the voltage drop, space-charge effect is another reason for the increase of charge collection time. Modelling of charge collection processes taking into account these two effects was done by V. Kubytskyi and explained in Ref. [**?**]. His simulations have shown that $V_{drop} \ll V_{bias}$ for less than 10^5 input electrons, and for $N_{CH} = 10^6$ the V_{drop} is estimated to be $\sim 25V$, which still does not strongly affect on the charge collection dynamics. However, when $N_{CH} > 10^6$ the signal V_{drop} reach values even larger than V_{bias}, which is unphysical and contradictory with our measured signals, therefore, V_{drop} at maximum can reach the values close to V_{bias} (see Fig. 7.25 (b).

The second campaign of measurements was carried out on 20th Dec.2014. Fig. 7.26 (a) shows the positions we have chosen to put the DSv during the measurements. The

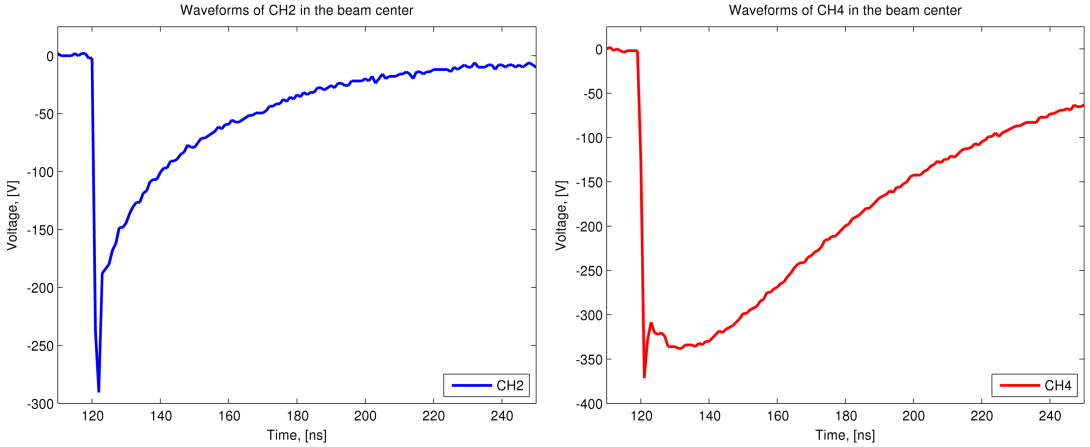

(a) **(b)**

Figure 7.25: Signal waveforms of CH2 (a) and CH4 (b) in the beam center with $V_{bias} = 400V$.

DSv was moved to 4 positions (A and B)with 2 mm distance from each other. The positions were chosen not only to measure the linearity response of DSv, but also to compare the signal strength of different channels.

Fig. 7.26 (b) shows the measured linearity response of DSv at position A and B. From the figure it can be seen that at position A, as CH1 is centered CH4 has less charge collected, same behaviour for CH1 when CH4 is centred at position B. This behaviour is similar to the what we have observed from Fig. 7.23, however, as the beam intensity is 10 times higher, the correction factor may be higher than 20%. Corrections were done with 20% and 40% of the signal from the channel that is centred, the comparison of the signals with different correction factor is shown in the Fig. 7.26 (c and d). It can be seen that with 40% correction the data fits better than with 20% correction. After correction the data is quite consistent with the data taken on 12th Dec. 2014 (see Fig. 7.24) with the same saturation level at 10^7 electrons.

7.6 Summary

A DSv with large dynamic range was designed for beam halo measurements at ATF2. With the present design, the lower and upper dynamic range of the DSv are limited by the signal pick-up at the level of 10^3 electrons and by the non-linearity starts from 10^7 electrons, respectively. Besides, with proper calibration for the signal in the non-linear

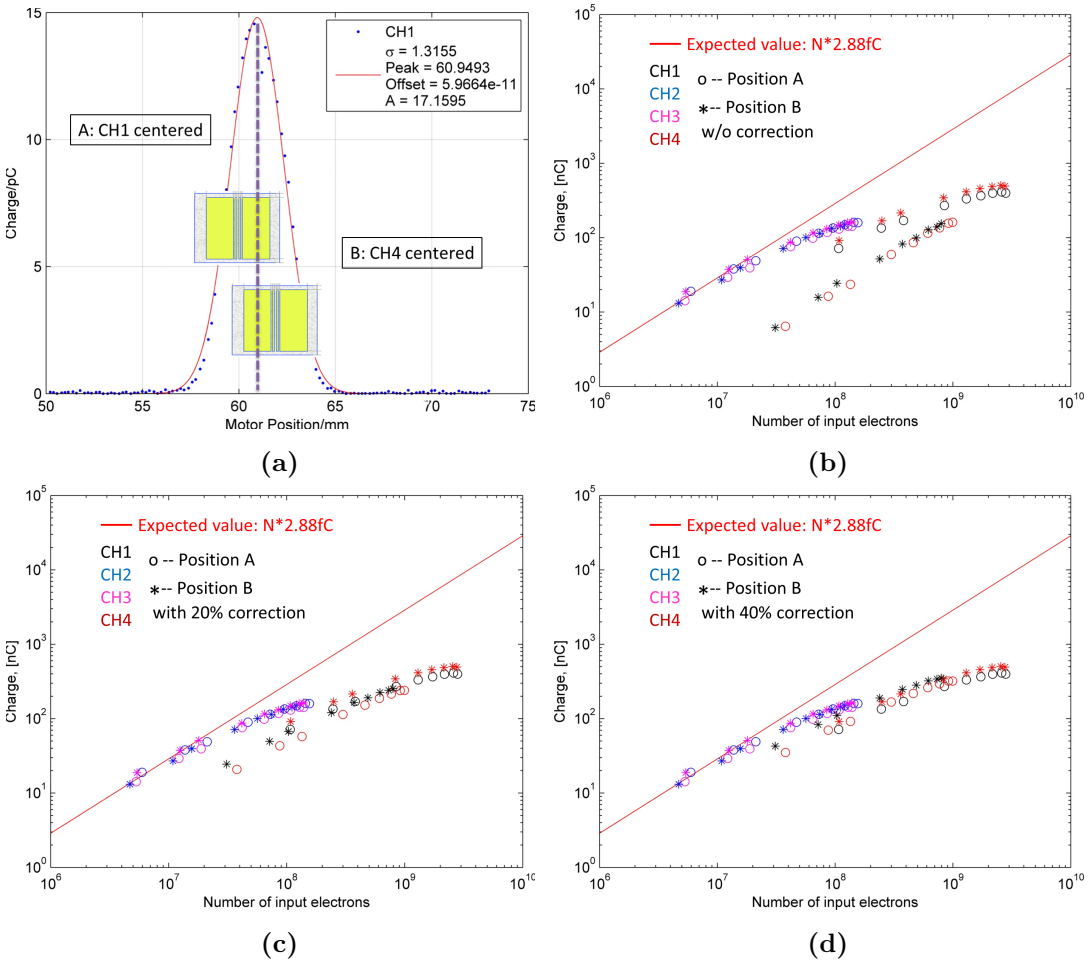

Figure 7.26: Scheme of measurement of CCE at different locations of beam core (a); Measurement results w/o correction (b), with 20% correction (c) and with 40% correction (d) (data taken on 20-12-2014 with BX100BY1000 Optics).

region, the upper limit of the dynamic range of DSv can be further extended (to $\sim 10^9$ in our experiment).

For the signal pick-up, a LPF in data analysis was used to recover the signal, besides, shielding of the PCB will be applied for the next set of the DSv. The non-linear response of the DSv due to large voltage drop on the 50 Ω resistor can be avoided by adding a smaller resistor. With these solutions, the dynamic range of the DSv can be further improved.